

# Analysis of Electron Confinement in Semiconductor (Ge, GaN, and ZnO) Quantum Nanowires

**Niloy Goswami**

Department of Electrical and Electronics Engineering, American International University-  
Bangladesh

**Nafisa Tabassum**

Department of Electrical and Electronics Engineering, American International University-  
Bangladesh

**Md. Redowan Habib**

Department of Electrical and Electronics Engineering, American International University-  
Bangladesh

**Md. Kabiruzzaman**

Department of Electrical and Electronics Engineering, American International University-  
Bangladesh

<https://doi.org/10.5109/7342435>

---

# Analysis of Electron Confinement in Semiconductor (Ge, GaN, and ZnO) Quantum Nanowires

Niloy Goswami<sup>1</sup>, Nafisa Tabassum<sup>1</sup>, Md. Redowan Habib<sup>1</sup>, Md. Kabiruzzaman<sup>1,\*</sup>

<sup>1</sup>Department of Electrical and Electronics Engineering, American International University-Bangladesh, 408/1 (Old KA 66/1), Kuratoli, Khilkhet, Dhaka 1229, Bangladesh

\*Author to whom correspondence should be addressed:

E-mail: kabiruzzaman@aiub.edu

(Received May 23, 2024; Revised December 13, 2024; Accepted January 7, 2025).

**Abstract:** Quantum nanostructures show promising applications in scaling electronic devices due to their exciting electronic and optical properties. In this work, a comparison of electron densities and confinement capabilities of nanowires made of three semiconductor materials (Ge, GaN, and ZnO) at low temperature ( $T = 10$  K) is done through numerical-based modeling. Numerical calculation is done using the Poisson-Schrödinger (PS) and Thomas-Fermi (TF) approximation equations through the finite element method. Physical phenomena of one-dimensional structures, e.g., charge density waves (CDW) and Friedel oscillations (FO) in these nanowires, have also been studied. Numerical analysis of electron densities and confining potentials exhibits FO in all of these Ge, GaN, and ZnO nanowires. Results showed that lower energy states having smaller values in azimuthal quantum number ( $m = 0, 1, 2$ ) contribute the most to carrier density profile. Finally, all three materials show Fermi-level-pinned energy that has great impact on the possibility of photogeneration gain.

Keywords: Nanowires; Friedel Oscillations; Electron Confinement; Carrier Density; Sub-band Energy

## 1. Introduction

Electronic devices, which consist of low-dimensional structures, are being studied currently to integrate them for the purpose of continuous down-scaling. Quantum dots, quantum wires, and quantum wells are examples of these low-dimensional structures. They are investigated a lot due to their promising and significant properties, which are different from their bulk counterpart. Semiconductor quantum wires, sometimes defined as nanowires (NWs) have shown significant interest due to their outstanding thermal, electrical, optical, chemical, and mechanical properties<sup>1-5</sup>. Electrical carriers in nanowires are confined in two directions that are perpendicular to each other. Physically, they have certain intriguing attributes that set them apart from both quantum dots and bulk materials<sup>6</sup>. Some examples of the interesting physical phenomena shown by nanowires are the quantization of electron states, charge density waves (CDW), Friedel oscillations (FO), and so on, which affect the transport properties. The quantization states of the energy levels can be used as logic functions, which can be used in the cutting-edge technology of qubits<sup>7</sup>. CDW study can help to understand the exciting physical properties for example, Wigner crystal formation<sup>8</sup>, Majorana physics in semiconductor<sup>9</sup>. Friedel oscillations are special types of standing waves

observed near impurities, disorders, or defects in one-dimensional (1D) systems. These types of characteristics are used to explore the band structure of the system in addition to hidden physics of the current quantum devices, for example, the chirality of the electrons in graphene, the wave-function structure in quantum Hall systems, or fundamental behavior of the underlying model describing high-temperature superconductors. Moreover, interesting and promising properties of topological insulators are also predicted to be explained using FO<sup>10</sup>. Some examples of theoretically calculated FO studies are Si dopants on GaAs surfaces<sup>11</sup>, GaAs NWs<sup>12</sup>, ZnO(101 $\bar{0}$ )<sup>13</sup> surface to bulk. Besides these theoretical modeling and calculations, experimental proof is also available to observe such types of sophisticated but exciting properties. For example, scanning tunneling microscopy (STM) images give the proof of FO around the defects in the sidewalls of GaN(101 $\bar{0}$ )<sup>14</sup>, Si-doped GaAs(110)<sup>15</sup>, Ir-induced nanowires on Ge(001)<sup>16</sup>, induced energy gap observed in epitaxial graphene growth on SiC(0001)<sup>17</sup>. Though all these studies are related to the FO observed around defects or impurities or charged ions on surfaces, detailed exploration of FO in nanowires itself is still uncovered and inevitable to understand the complete physics behind this.

In this paper, we considered equally doped nanowires of Ge, GaN, and ZnO separately in order to study the

possibility of FO. We considered these materials from their wide application in optoelectronics perspective. Ge is an optoelectronic semiconductor with a direct bandgap. Thermoelectric devices, which convert heat into electricity, have also been tested with Ge nanowires. Ge nanowires have a better thermoelectric figure of merit than bulk Ge because their greater surface area scatters phonons and improves the Seebeck coefficient<sup>18,19</sup>. Ge nanowires' direct bandgap and high absorption coefficient make them good photodetectors. High-speed optical communications use Ge nanowire photodetectors because of their high responsivity and fast reaction time<sup>20</sup>.

Nitride semiconductor materials, such as GaN, have consistently garnered a great deal of interest over the course of the past two decades due to the superior optical and electronic properties that they possess. These properties include a wide band gap that can be adjusted, strong atomic bonds, and high thermal stability<sup>21,22</sup>. GaN's direct bandgap of 3.4 eV makes it a desirable material for UV photodetection applications due to the semiconductor's excellent efficiency at absorbing UV light. GaN can also function at high temperatures because of its high melting point. These characteristics recommend GaN for application in high-reliability, high-performance electrical and optoelectronic devices. The semiconductor zinc oxide (ZnO) is quite promising for a variety of optical applications. It has performed well in UV detectors, lasers, solar cells, and light-emitting diodes (LEDs)<sup>23-25</sup>. Ren et al. reported that the photocurrent of a ZnO nanowire (NW) increased with its length, attributed to a mean free path effect resulting in a unique distribution of dark electron density along the length. This study provides valuable insights into the length-dependent photoelectric behavior of ZnO NWs, contributing to the advancement of the field<sup>26</sup>. Movlaroooy et al. investigated the structural, electronic properties, and quantum confinement effects of zinc oxide (ZnO) nanotubes and nanowires with different diameters, utilizing density functional theory and the pseudopotential approximation. The results demonstrate that reducing the diameter of ZnO nanotubes and nanowires leads to an increased energy gap, making them promising candidates for nanoscale optoelectronic devices due to their direct band gap and size-dependent properties<sup>27</sup>. Research on electron confinement in semiconductor quantum structures has advanced, particularly regarding the effects of external fields and material compositions. For instance, studies have explored how hydrostatic pressure, and electric fields impact the binding energy of donor impurities in GaAs quantum dots<sup>28,29</sup>. Additionally, the interplay between structural dimensions and external influences has been shown to affect the density of states and polarizability in GaAs-(Ga, Al)As quantum wells<sup>30</sup>. Furthermore, the unique optical and electronic properties of GaAs-Al<sub>x</sub>Ga<sub>1-x</sub>As quantum dots reveal how impurities and external fields can enhance these characteristics, emphasizing the significance of material selection and

configuration in nanowire applications<sup>31</sup>). These findings provide valuable insights for optimizing electron confinement in Ge, GaN, and ZnO nanowires for future electronic and optoelectronic devices. Collectively, these studies highlight the critical role of understanding electron dynamics in advancing nanostructured semiconductor technologies.

In this work, the carrier density profiles, and confining potentials were calculated for three semiconductor nanowires made of Ge, GaN, and ZnO to investigate the possibility of having the Friedel oscillations. The computation exhibits the FO in all of these Ge, GaN, and ZnO nanowires. Moreover, the calculated electron potentials for the surface states of all three materials show Fermi-level-pinned energy. The radial effect of the Carrier density profile, confining potential, as well as the origin of FO in the cylindrical nanowires of these three materials, has been discussed.

The paper is organized in the following way: In Section 2, a mathematical model of the electron confinement in the quantum nanowire is described. The results of a case-by-case comparison of electron confinement in quantum nanowires based on three different semiconductor materials (Ge, GaN, and ZnO) are presented with discussion in Section 3. Lastly, Section 4 provides some conclusive findings along with future possibilities for the outcome.

## 2. Numerical model

A commercial COMSOL-Multiphysics software includes the interface for the Schrödinger-Poisson (SP) equation, which is utilized in the simulations presented in this paper<sup>17,32</sup>. To visualize the band formation and energy levels in a nanowire, it is important to find a solution to the Schrödinger equation that describes the system.

$$\sum_{n=1}^N H_{mm} \psi_m^{(i)}(r) = E \psi_m^{(i)}(r) \quad (1)$$

here, specific quantum mode or state,  $m = 1, 2, 3, 4, \dots, N$ . [ $N$  = number of wave function elements],  $H_{mm}$  Hamiltonian matrix element for a specific state  $m$  can be written as  $H_{mm} = \frac{\hbar}{2m^*} \nabla^2 + V(r)$ ,  $\hbar$  is the reduced Planck constant,  $m^*$  is the electron's effective mass,  $\nabla^2$  represents the Laplacian, contributing to the kinetic energy term,  $V(r)$  is the potential energy at position  $r$ ,  $E$  is the energy eigenvalue associated with mode  $m$ ,  $\psi_m^{(i)}(r)$  denotes the wavefunction of mode  $m$  for the  $i$ -th configuration, at position  $r$ . This Hamiltonian governs both the kinetic and potential energy contributions for each quantum state  $m$  in the nanowire system. A comprehensive flowchart that illustrates the step-by-step self-consistent solution process of the Schrödinger-Poisson equations within a specific quantum nanowire system is depicted in Fig. 1. Solving Poisson's equation gives the iterations, which can be considered as an

excellent start. To calculate the electric potential  $V$ , the following equation is used:

$$-\nabla \cdot (\epsilon \nabla V) = \rho_s \quad (2)$$

where the symbol  $\epsilon$  represents permittivity, and the symbol  $\rho_s$  represents space charge density, which is considered the best initial estimate using the Thomas-Fermi (TF) approximation<sup>32</sup>. The Thomas-Fermi approximation is suitable for the initial charge density estimation due to its computational efficiency and accuracy, particularly in highly doped nanowires. It provides a quick response to potential changes, making it ideal for starting self-consistent calculations. Alternatives like the Poisson-Boltzmann distribution or DFT can be used, but they are more computationally demanding. In the second step, the potential energy,  $V_e$  component in the Schrödinger equation is affected by the electric potential,  $V$ ,  $q$  is the magnitude of the charge of the electron, approximately  $1.602 \times 10^{-19}$  coulombs.

$$V_{e=} - qV \quad (3)$$

Equation (4) describes the particle density profile,  $n_{\text{sum}}$ , as a statistical sum of probability densities weighted by the occupancy factors  $N_i$ . The relationship between the particle density and the potential energy is established by considering the Schrödinger equation, which is a fundamental equation in quantum mechanics governing the behavior of particles at the quantum level,

$$n_{\text{sum}} = \sum_i g_i \left( \frac{2m_e}{\pi \hbar^2} \right)^2 (k_B T)^{1/2} F_{-1/2} \left( \frac{E_f - E_i}{k_B T} \right) |\psi_i|^2 \quad (4)$$

Since the electrons must remain within the quantum wire, it is required to apply the boundary condition,  $\psi(\Omega) = 0$  (where  $\Omega$  defines boundaries for all cases) in order to find a solution to this equation. where  $i$  signifies the number of iterations that contributes to the summation. The formulation of this equation (4) is based on Fermi-Dirac statistics, which describe the distribution of particles over energy states in a system of indistinguishable fermions. In this equation (4):

- $g_i$ : Represents the degeneracy factor for the  $i$ -th energy level, accounting for the number of available states at that energy level in the nanowire. This factor is typically calculated based on the effective mass and dimensionality of the system.
- $(k_B T)^{1/2}$ : Arises from the thermal energy contribution, which is significant in low-temperature scenarios where thermal excitations influence the occupancy of quantum states.
- $F_{-1/2}$ : This term is the Fermi-Dirac distribution function, describing the occupancy of energy levels at a given temperature  $T$  and Fermi

energy  $E_f$ .

- The occupancy of states is influenced by the energy difference  $E_f - E_i$ , and the exponential decay of occupancy at energies significantly higher than the Fermi level reflects the statistical nature of fermions.

Recalculating the space charge density and utilizing it to solve Poisson's equation again results in a new electric potential profile based on the particle density profile,  $n_{\text{sum}}$ . This provides an accurate representation of the electric potential profile. The new space charge density is<sup>33</sup>,

$$\rho = q n_{\text{sum}} \quad (5)$$

This indicates the divergence of the iterations. The recalculated space charge density  $\rho$  results in a new electric potential profile that may differ significantly from previous iterations. Such divergence occurs when the differences between new and old values of electric potential  $V$  exceed the specified convergence tolerance, indicating the need for further iterations to achieve stability in the self-consistent solution process. A better expression can be written as

$$\rho = q n_{\text{sum}} \exp \left( e^{-\alpha \frac{-q(V-V_{\text{old}})}{k_B T}} \right) \quad (6)$$

where  $V_{\text{old}}$  represents the previous iteration's electric potential and  $\alpha$  is an extra tuning parameter. The value of  $\alpha = 0$  for high temperatures whereas some positive values of  $\alpha$  works well for low temperatures. The solver sequence uses this equation to determine the space charge density,  $\rho$  which is further used to determine the new electric potential,  $V$ . This process is continued until the tolerable difference between old and electric potentials,  $V_{\text{old}}$  and  $V_{\text{new}}$ , respectively, is reached. Thus, self-consistency is achieved. Equation (6) is derived from modifying the basic charge density equation (5) to account for temperature effects and potential changes more effectively. It incorporates an exponential factor that helps mitigate numerical instability during iterative calculations, particularly in low-temperature scenarios where charge distributions can vary significantly.

In this study, 50 nm radius of quantum nanowire is selected for the study of quantum confinement and feasibility for current fabrication. The results are investigated in 10 K to minimize thermal energy and observe discrete electron states. The electron effective mass and dielectric constant differ for each material, as outlined in Table 1. These choices are crucial for detailed studies of electron confinement in nanowires. The nanowire is modeled as having cylindrical symmetry and a 1D axisymmetric space dimension. To avoid edge effects and ensure that electron confinement is primarily radial,

the nanowire is assumed to be infinitely long. The material compositions considered are Ge, GaN, and ZnO, with a consistent doping concentration of  $2.6 \times 10^{18} \text{cm}^{-3}$ . These

properties are selected to allow a direct comparison of electron density and confinement effects across different semiconductor materials.

Table 1. Modelling parameters of semiconductor materials.

Parameters [unit]/Materials	Ge	GaN	ZnO
Radius [nm]	50	50	50
Energy Bandgap [eV]	0.7	3.4	3.37
Electron Effective Mass	$0.12m_e$	$0.13m_e$	$0.28m_e$
Dielectric Constant	16.2	8.9	8.66
Electron Doping [ $\text{cm}^{-3}$ ]	$2.6 \times 10^{18}$	$2.6 \times 10^{18}$	$2.6 \times 10^{18}$
Temperature [K]	10	10	10
References	18),37)	38)	34),39)

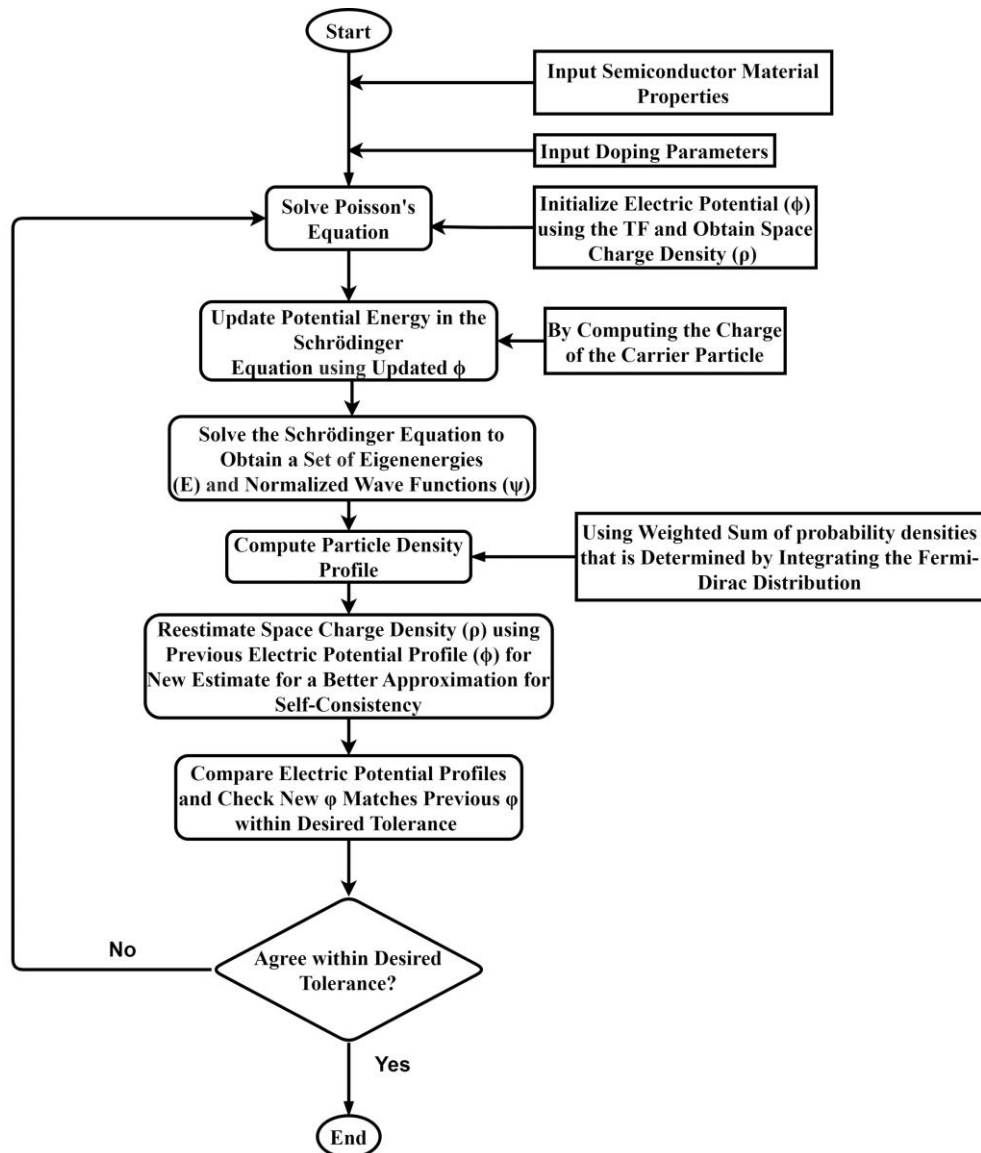


Fig. 1: Flowchart for self-consistent solution process of the schrödinger-poisson equations.

### 3. Results and discussions

The computational results obtained for carrier density profiles and confining potentials for Ge nanowires are illustrated in Fig. 2. The left ordinate axis of Fig. 2(a) shows the electron density functions

normalized by the donor density. The carrier density profiles are obtained from the Thomas-Fermi approximation (shown in a smooth line) and the PS equation (shown in an oscillatory line). The confining potential shown in the dashed dot lines corresponds to

the right ordinates.

For the Ge, the confining potential is almost independent of cylindrical nanowire radius up to 30 nm with a value nearly equal to its charge-neutral flat band value. In the TF approximation, the quantization effects in energy density, sub-bands in lower temperature (here,  $T = 10$  K), and lower number of eigenstates near the center were ignored, contributing to a non-oscillatory line. However, considering those effects in PS calculation results in the oscillatory curves. The oscillations on the electron density profiles were calculated as the individual contribution of azimuthal quantum numbers ( $m$ ). These oscillations are also denoted as so-called Friedel-type spatial oscillations obtained from Poisson-Schrodinger results. The local maxima of oscillations are shown in vertical dashed lines drawn through the points of (1), (2), and (3). The contributions of components of electronic states in the density maximas are summarized in Table 2. For point 1, as shown in Fig. 2(a) and Table 2, maximum contributions come from state ( $m=1$ ), which is  $\sim 41\%$  and the second highest contributions come from  $m=2$  state.

Besides the contributions from  $m=0, 1$ , and  $2$  are significant, others have less than  $10\%$  in the carrier density profiles. Hence, this oscillation in point 1 appeared for lower states, particularly  $m$  is less than  $3$ . This type of lower states contributed oscillation in carrier density profiles are also seen in the case of GaAs<sup>12</sup>. For the point 2 oscillations located at the distance of  $17$  nm from the center, the maximum contributions come from the  $m=2$  state having a value of  $24.24\%$ . The second and third highest contributions are obtained from  $m=1$  and  $3$  states corresponding values of  $\sim 22\%$  and  $18\%$ , respectively. In the case of third oscillations centered at  $r = 24$  nm, the contributions are almost equal from the middle states, which are around  $\sim 20\%$ . Additionally, the amounts from the lower states  $\sim 10\%$  including the lowest value

which is  $9.84\%$ . Hence, we can conclude here, the oscillation nearest to the center is due to lower states, middle oscillations can be summed over intermediate states and farthest oscillations are obtained from the highest occupied states. The probability densities of the carriers having the largest contributions in the first two oscillations are given in Fig. 2(b), where the electrons of lower energy states are accumulated mostly near the center. For higher values of  $m$ , the peaks are farther away from the central axis. All above results give the conclusion that the electrons having lower occupied states are located near the center, whereas the electrons having higher occupied states are accumulated farther from the center in the range of  $15$  to  $30$  nm for the Ge nanowires.

Table 2. Contribution of each state in percentage for (1), (2) and (3).

Nanowire Material	$m$	$P_1$ (%)	$P_2$ (%)	$P_3$ (%)
Ge	0	19.24	11.55	9.84
	1	41.38	21.99	20.92
	2	29.20	24.24	20.71
	3	7.81	18.31	18.87
	4	1.76	16.35	17.36
	5	0.61	7.55	12.29
GaN	0	96.32	17.51	7.55
	1	3.66	36.81	23.68
	2	0	27.36	25.62
	3	0	9.98	21.08
	4	0	4.79	14.48
	5	0	3.33	7.55
ZnO	0	14.44	1.59	0.87
	1	47.33	22.24	20.98
	2	27.96	31.82	20.70
	3	6.26	24.44	20.91
	4	3.18	17.05	20.31
	5	0.82	2.54	16.22

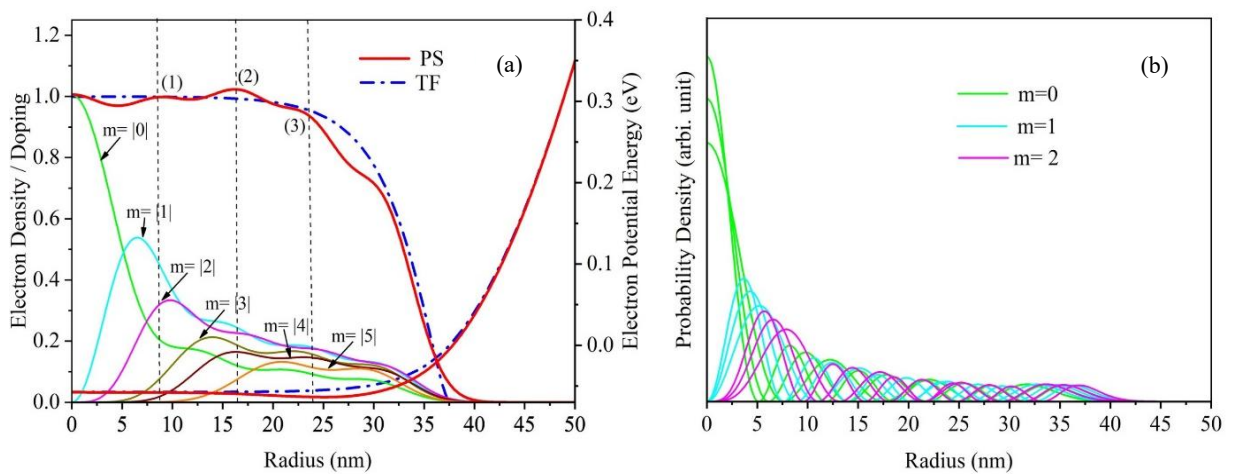
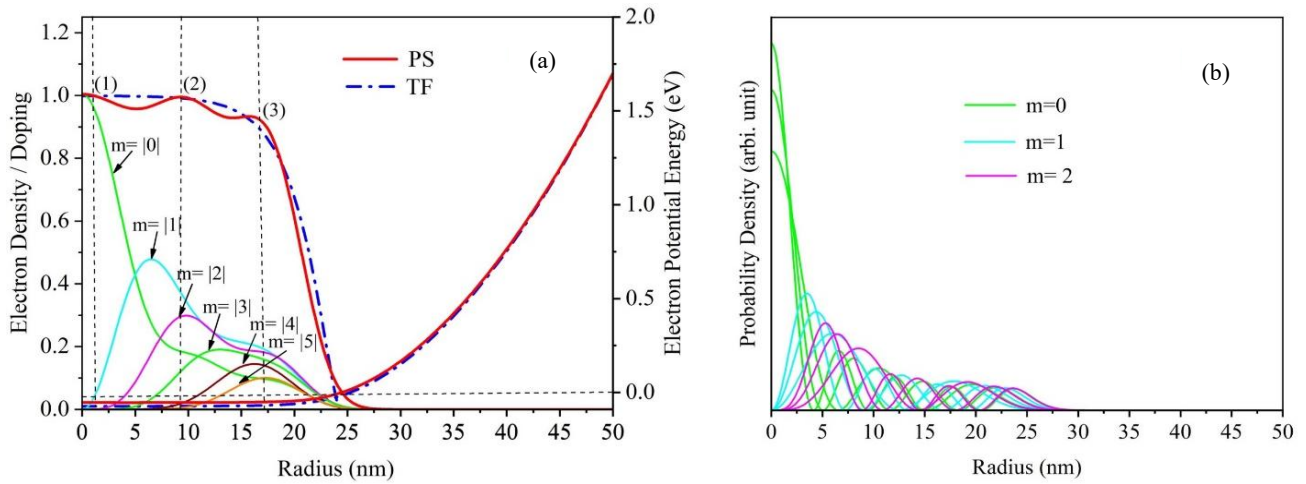


Fig. 2: Ge: (a) Electron density profiles normalized with doping concentration ED with doping and electron potential energy (EPE), (b) Probability density for different azimuthal numbers ( $m$ ).

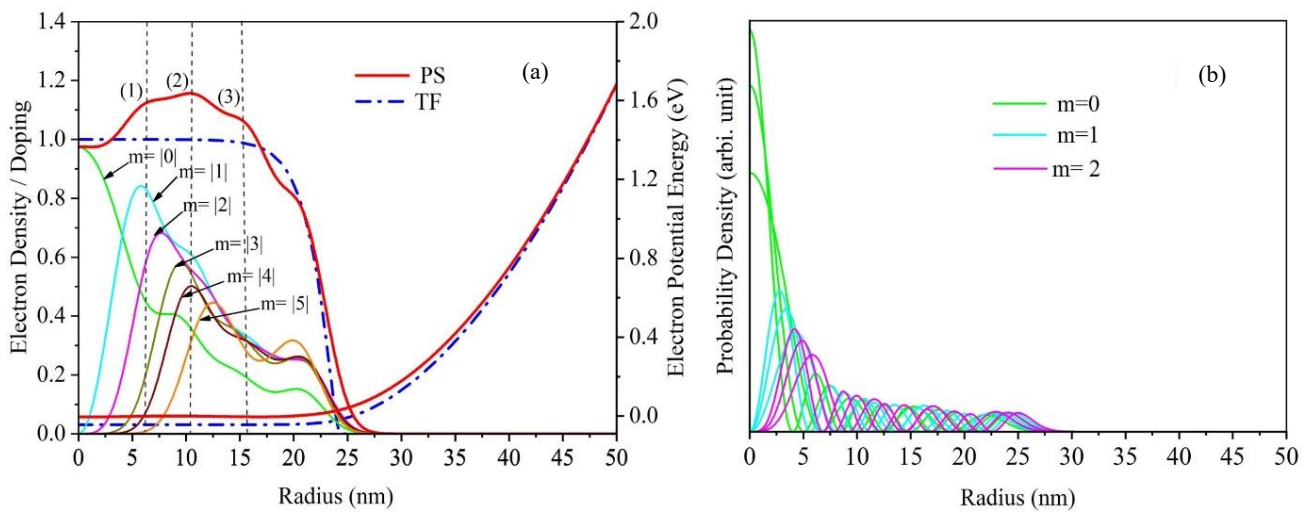
The radial distribution of electron density function and confining potentials are shown in Fig. 3 and 4 for the cases of GaN and ZnO, respectively. Each figure demonstrates carrier probability distributions which also have contributions in the oscillations. The contributions from individual  $m$  are demonstrated in the percentage in Table 2. For GaN, as shown in Fig. 3(a), there is no contribution of the first two  $m$  values. For the second oscillation, the first three  $m$  values have made above 30% while the last three  $m$  values have made less than 10%. In the case of the third oscillation, all the  $m$  values have contributed around 20% except the 1st and last ones which have contributed less than 10%. Figure 3(b) shows the probability densities which prove again that the states having lower energy are in the center. The peaks for higher energy states are farther away from the center. The confining potential plot indicates the depletion of states from the center and pinned at the surface at the value half of the band gap which is

$\sim 1.70 \text{ eV}^{34}$ .

The electron density function for ZnO has been shown in Fig. 4(a) along with the probability density function in Fig 4(b). The percentage contributions of the states in the density profile are shown in Table 2. For the first oscillation, the maximum contribution is 47% whereas gradual decreasing of  $\sim 31\%$  and  $\sim 21\%$  are for the 2nd and third oscillations, respectively. It's worthwhile mentioning, even though the average contributions for these 6 states are around 20% for the 3rd oscillation, for the first oscillations last three states have contributions of less than 10%. The confining potential plot indicates the depletion of states from the center and pinned at the surface at the value half of the band gap, which is  $\sim 1.69 \text{ eV}^{35}$ . Like Ge and GaN, ZnO also shows that the non-zero angular momentum states are accumulated at the interior of the cylindrical quantum wire.



**Fig. 3:** GaN: (a) Electron density profiles normalized with doping concentration and electron potential energy (EPE), (b) Probability density for different azimuthal numbers ( $m$ ).



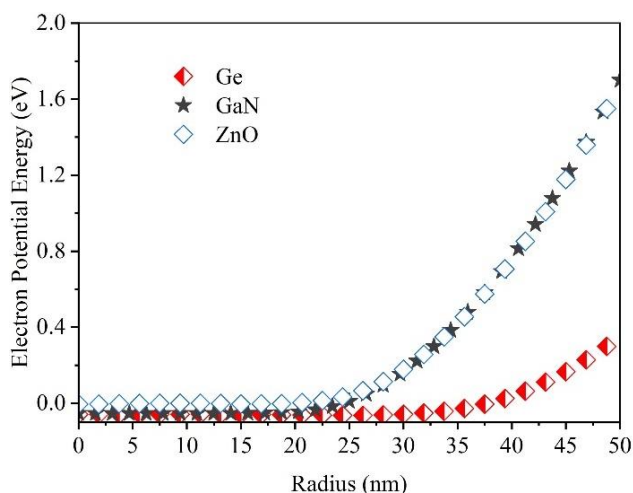
**Fig. 4:** ZnO: (a) Electron density profiles normalized with doping concentration and electron potential energy (EPE), (b) Probability density for different azimuthal numbers ( $m$ ).

Figure 5 shows the comparison of the potential energy of these three materials with respect to radius. The

potential energy can be related to one of the surface effects i.e. surface band bending (SBB). SBB can be defined as

the bending of the conduction layers at the surface from/towards the Fermi level based on the doping type. This type of surface effect significantly affects the optical properties of nanowires, e.g., photoresponsivity, photocarrier relaxations, and so on. The SBB for Ge, GaN and ZnO are 0.35, 1.7 and 1.69, respectively which are obtained from surface Fermi-level-pinned energy. Since 0.3 eV is strong enough radial field for Ge NWs<sup>36</sup>, it can be used for the separation of photogenerated carriers, which in turn enhances the photo-gain of optoelectronic devices. This generalization is true for GaN and ZnO NWs as well.

The comparative analysis of electron potential energy as a function of radius among Ge, GaN, and ZnO nanowires aims to highlight the distinct confinement characteristics of each material. These variations in potential energy directly influence the carrier confinement and spatial distribution of electron density, which are crucial for determining the material's suitability for optoelectronic applications. For instance, stronger confinement (as observed in materials with higher potential energy variation) can lead to enhanced quantum efficiency in devices like quantum dot lasers or photodetectors. This analysis will provide insights to see which material might be better suited for specific applications based on the desired confinement properties and operating conditions.



**Fig. 5:** Comparison plot for three materials. Electron potential energies of three materials with respect to radius showing Fermi-level-pinned energy which has great impact in the photogenerations gain.

#### 4. Conclusion

This paper describes a computational approximation for electron confinement in quantum nanowires of Ge, GaN, and ZnO with Fermi-level-pinning boundary conditions and the coupled Poisson and Schrödinger models of the electron states. Low-temperature ( $T = 10$  K) effects of the carrier density profile, and electron potentials show Friedel oscillations. This FO can be attributed to the completely depleted or smaller number of sub-bands.

Among different oscillations, the contributions of the azimuthal quantum numbers have also been shown here. The numerical results illustrated that the quantum numbers nearest to the center have higher contributions. The radial dependence of electron potentials has been demonstrated here. This electron potential gives the surface band bending for all three nanowires, which can be considered enough potential energy for photogeneration gain. This study is the groundwork for investigating the physical phenomena in the low-dimensional structures (here NWs) that can be considered for obtaining the crucial and beneficial transport properties. Moreover, this work can enhance the understanding of the electron confinement behavior of semiconductor materials in nanowires, which could be important in developing the next generation of quantum electronics.

#### Data Availability

The corresponding author can provide the data used in the study upon request.

#### Conflicts of Interest

The authors confirm that there is no conflict of interest associated with the publication of this paper.

#### Acknowledgements

The authors would like to acknowledge the Department of Electrical and Electronics Engineering at American International University-Bangladesh for their full support. We are also grateful to Dr. Mainul Hossain and Dr. Rezwana Ahmed for critical reading of this manuscript.

#### References

- 1) B. M. Wong, C. Chevalier, "HADOKEN: An open-source software package for predicting electron confinement effects in various nanowire geometries and configurations", *Computer Physics Communications*. 274, 108299–108299 (2022). <https://doi.org/10.1016/j.cpc.2022.108299>.
- 2) Z. Wu, J. B. Neaton, J. C. Grossman, "Quantum Confinement and Electronic Properties of Tapered Silicon Nanowires", *Physical review letters*, 100 (24), 246804 (2008). <https://doi.org/10.1103/physrevlett.100.246804>.
- 3) Y. Cui, C. M. Lieber, Functional Nanoscale Electronic Devices Assembled Using Silicon Nanowire Building Blocks, *Science*. 291 (5505), 851–853 (2001). <https://doi.org/10.1126/science.291.5505.851>.
- 4) Y. Huang, X. Duan, Q. Wei, C. S. Lieber, "Directed Assembly of One-Dimensional Nanostructures into Functional Networks", *Science*. 291, (5504), 630–633 (2001). <https://doi.org/10.1126/science.291.5504.630>.

- 5) M. I. den Hertog, F. González-Posada, R. Songmuang, J. L. Rouviere, T. Fournier, B. Fernandez, E. Monroy, "Correlation of Polarity and Crystal Structure with Optoelectronic and Transport Properties of GaN/AlN/GaN Nanowire Sensors", *Nano Letters*. 12 (11), 5691–5696 (2012). <https://doi.org/10.1021/nl302890f>.
- 6) X. Zhao, C. M. Wei, L. Yang, M. Y. Chou, "Quantum Confinement and Electronic Properties of Silicon Nanowires", *Physical Review Letters*. 92 (23), 236805(2004).<https://doi.org/10.1103/physrevlett.92.236805>.
- 7) K. Pomorski, P. Giouanlis, E. Blokhina, D. Leipold, P. Pęczkowski, R. B. Staszewski, "From two types of electrostatic position-dependent semiconductor qubits to quantum universal gates and hybrid semiconductor-superconducting quantum computer", *Superconductivity and Particle Accelerators*. 11054, 47–166 (2019). <https://doi.org/10.1117/12.2525217>.
- 8) A. Rahman, M. K. Sanyal, "Observation of charge density wave characteristics in conducting polymer nanowires: Possibility of Wigner crystallization", *Physical Review B*, 76 (4), 045110 (2007). <https://doi.org/10.1103/physrevb.76.045110>.
- 9) B. D. Woods, S. D. Sarma, T. D. Stanescu, "Subband occupation in semiconductor-superconductor nanowires", *Physical Review B*, 101 (4), 045405 (2020). <https://doi.org/10.1103/physrevb.101.045405>.
- 10) C. Bena, "Friedel oscillations: Decoding the hidden physics", *Comptes Rendus Physique*, 17 (3–4), 302–321(2016).<https://doi.org/10.1016/j.crhy.2015.11.006>.
- 11) J. E. Inglesfield, M. H. Boon, S. Crampin, "Nature of Friedel oscillations around Si dopants in the GaAs(110) accumulation layer", *Journal of Physics: Condensed Matter*, 12 (30), L489–L496 (2000). <https://doi.org/10.1088/0953-8984/12/30/102>.
- 12) J. H. Luscombe, A. M. Bouchard, M. Luban, "Electron confinement in quantum nanostructures: Self-consistent Poisson-Schrödinger theory", *Physical Review B*. 46 (16), 10262–10268 (1992). <https://doi.org/10.1103/physrevb.46.10262>.
- 13) H. Hu, Z. Lv, S. Cui, G. Zhang, "Theoretical study of ZnO(101 $\bar{0}$ ) and M/ZnO(101 $\bar{0}$ ) ", *Chemical Physics Letters*. 510 (1–3), 99–103 (2011). <https://doi.org/10.1016/j.cplett.2011.05.009>.
- 14) E. G. Banfi, T. J. F. Verstijnen, E. Monroy, M. E. Flatté, P. M. Koenraad, "Atomically resolved study of the unpinned GaN ( 101 $\bar{0}$  ) surface by cross-sectional scanning tunneling microscopy", *Physical review*. 108, (8), 085304 (2023). <https://doi.org/10.1103/physrevb.108.085304>.
- 15) M. C. M. van der Wielen, A. J. A. van Roij, H. van Kempen, "Direct observation of Friedel oscillations around incorporated sie, dopants in GaAs by low-temperature scanning tunneling microscopy", *Physical Review Letters*. 76 (7), 1075–1078 (1996). <https://repository.ubn.ru.nl/handle/2066/28500>.
- 16) T. F. Mocking, P. Bampoulis, N. Oncel, B. Poelsema, H. J. W. Zandvliet, "Electronically stabilized nanowire growth", *Nature Communications*. 4 (1) (2013). <https://doi.org/10.1038/ncomms3387>.
- 17) K. Clark, X.-G. Zhang, G. Gu, J. Park, G. He, R. M. Feenstra, A. Li, "Energy Gap Induced by Friedel Oscillations Manifested as Transport Asymmetry at Monolayer-Bilayer Graphene Boundaries", *Physical Review X*. 4 (1) (2014). <https://doi.org/10.1103/physrevx.4.011021>.
- 18) S. Prucnal, F. Lui, M. Voelskow, L. Vines, L. Rebohle, D. Lang, Y. Berencén, S. Andric, R. Boettger, M. Helm, S. Zhou, W. Skorupa, "Ultra-doped n-type germanium thin films for sensing in the mid-infrared", *Scientific Reports*. 6 (1) (2016). <https://doi.org/10.1038/srep27643>.
- 19) S.M. Yang, L.A. Chung, H. R. Wang, "Review of polysilicon thermoelectric energy generators", *Sensors and Actuators A: Physical*. 346, 113890–113890 (2022). <https://doi.org/10.1016/j.sna.2022.113890>.
- 20) S. An, S. Wu, K. Lee, C. S. Tan, Y. Tai, G. Chang, M. Kim, "High-Sensitivity and Mechanically Compliant Flexible Ge Photodetectors with a Vertical p–i–n Configuration", *ACS applied electronic materials*. 3 (4), 1780–1786 (2021). <https://doi.org/10.1021/acsaelm.1c00054>.
- 21) L. Zhang, J. Shi, Q. Wang, "Fröhlich electron–phonon interaction Hamiltonian and potential distribution of a polar optical phonon mode in wurtzite nitride triangular nanowires", *Journal of Applied Physics*. 132 (1) (2022) <https://doi.org/10.1063/5.0092503>.
- 22) Y. Ra, R. Navamathavan, S. Kang, C.R. Lee, "Different characteristics of InGaN/GaN multiple quantum well heterostructures grown on m- and r-planes of a single n-GaN nanowire using metalorganic chemical vapor deposition", *Journal of Materials Chemistry C*. 2 (15), 2692–2692 (2014). <https://doi.org/10.1039/c3tc32212b>.
- 23) Q. Yan, X. Guo, W. Wang, Y. Zhang, S. Xu, D. H. Lien, Z. L. Wang, "Enhancing Sensitivity of a Single ZnO Micro-Nanowire Photodetector by Piezophototronic Effect", *ACS Nano*. 4 (10), 6285–6291 (2010). <https://doi.org/10.1021/nn1022878>.
- 24) A. Chakraborty, A. Orsini, J. P. Kar, F. Gatta, U. Khan, C. Falconi, "Ultra-efficient thermo-convective solution-growth of vertically aligned ZnO nanowires", *Nano Energy*. 97, 107167–107167(2022). <https://doi.org/10.1016/j.nanoen.2022.107167>.
- 25) N. Gagrani, K. Vora, L. Fu, C. Jagadish, H. H. Tan, "Flexible InP–ZnO nanowire heterojunction light emitting diodes", *Nanoscale horizons*. 7 (4), 446–454 (2022). <https://doi.org/10.1039/d1nh00535a>.
- 26) R. Ren, X. Ren, Hao Liu, Y. Huang, W. Yuan," Length-Dependent Photoelectric Property of ZnO

- Nanowires”, *Nanoscale Research Letters*. 17 (1) (2022). doi: <https://doi.org/10.1186/s11671-022-03715-2>.
- 27) T. Movlaroooy, “Study of quantum confinement effects in ZnO nanostructures”, *Materials Research Express*. 5 (3), 035032 (2018). <https://doi.org/10.1088/2053-1591/aab389>.
- 28) C.M. Duque, M.G. Barseghyan, and C.A. Duque, “Donor impurity in vertically-coupled quantum-dots under hydrostatic pressure and applied electric field,” *Eur. Phys. J. B*, 73, 309–319 (2010). <https://doi.org/10.1140/epjb/e2009-00433-7>.
- 29) M.G. Barseghyan, A.A. Kirakosyan, and C.A. Duque, “Hydrostatic pressure, electric and magnetic field effects on shallow donor impurity states and photoionization cross section in cylindrical GaAs–Ga<sub>1-x</sub>Al<sub>x</sub>As quantum dots,” *Phys. Status Solidi B*, 246(3), 626–629 (2009). <https://doi.org/10.1002/pssb.200880516>.
- 30) A.L. Morales, A. Montes, S.Y. López, N. Raigoza, and C.A. Duque, “Donor-related density of states and polarizability in a GaAs-(Ga, Al)As quantum-well under hydrostatic pressure and applied electric field,” *Phys. Status Solidi C*, 2, 652–656 (2003). <https://doi.org/10.1002/pssc.200306176>.
- 31) C. Heyn, and C.A. Duque, “Donor impurity related optical and electronic properties of cylindrical GaAs–Al<sub>x</sub>Ga<sub>1-x</sub>As quantum dots under tilted electric and magnetic fields,” *Sci. Rep.*, 10(1), 9155 (2020). <https://doi.org/10.1038/s41598-020-65862-9>
- 32) C. Liu, “Self-Consistent Schrödinger-Poisson Results for a Nanowire Benchmark,” COMSOL, Oct. 18, 2018. <https://www.comsol.com/blogs/self-consistent-schrodinger-poisson-results-for-a-nanowire-benchmark>. (Last Accessed: 29 Mar. 2024)
- 33) J. A. Gil-Corrales, J.A. Vinasco, A. Radu, R. L. Restrepo, A. L. Morales, M.E. Mora-Ramos, C. A. Duque, “Self-Consistent Schrödinger-Poisson Study of Electronic Properties of GaAs Quantum Well Wires with Various Cross-Sectional Shapes”, *Nanomaterials*. 11 (5), 1219–1219 (2021). <https://doi.org/10.3390/nano11051219>.
- 34) Y. Yang, W. Guo, X. Wang, Z. Wang, J. Qi, Y. Zhang, “Size Dependence of Dielectric Constant in a Single Pencil-Like ZnO Nanowire”, *Nano Letters*. 12 (4), 1919–1922(2012). <https://doi.org/10.1021/nl204353t>.
- 35) Q. Wu, G. Liu, H. Shi, B. Zhang, J. Ning, T. Shao, S. Xue, F. Zhang, “Impact of Nd Doping on Electronic, Optical, and Magnetic Properties of ZnO: A GGA + U Study”, *Molecules*. 28 (21), 7416–7416 (2023). <https://doi.org/10.3390/molecules28217416>.
- 36) S. Sett, A. K. Raychaudhuri, “Effective Separation of Photogenerated Electron–Hole Pairs by Radial Field Facilitates Ultrahigh Photoresponse in Single Semiconductor Nanowire Photodetectors”, *Journal of Physical Chemistry C*. 124 (41), 22808–22816 (2020). <https://doi.org/10.1021/acs.jpcc.0c06582>.
- 37) Ghosh, S., Leonhardt, D., & Han, S. M.” Effect of threading dislocation density and dielectric layer on temperature-dependent electrical characteristics of high-hole-mobility metal semiconductor field effect transistors fabricated from wafer-scale epitaxially grown p-type germanium on silicon substrates”. *Journal of Applied Physics*, 115(9) (2014). <https://doi.org/10.1063/1.4867518>
- 38) S. Lakshman, K. Gazeli, Swaminathan, P., L. Invernizzi, Pere, Lombardi, G., & K. Ouaras. “Gallium nitride deposition via magnetron sputtering: Linking plasma-surface interactions and thin film crystalline features”. *Vacuum*, 224, 113185–113185 (2024). <https://doi.org/10.1016/j.vacuum.2024.113185>
- 39) Zeng, Z., Paspalakis, E., Garoufalos, C. S., Terzis, A. F., & Sotirios Baskoutas. Optical susceptibilities in singly charged ZnO colloidal quantum dots embedded in different dielectric matrices. *Journal of Applied Physics*, 113(5) (2013). <https://doi.org/10.1063/1.4789363>